A Wiener–Hopf-Type Analysis of Uniaxial Substrate–Superstrate Microstrip Structures

George A. Kyriacou, *Member, IEEE,* and John N. Sahalos, *Senior Member, IEEE*

***Abstract*—A Wiener–Hopf-type technique in conjunction with the hybrid-mode analysis and a space-domain Fourier transform pair was employed for the solution of the canonical problem of a TEM wave obliquely incident upon the edge and defined by a semi-infinite plate conductor lying at the interface of two uniaxial dielectrics, forming an otherwise grounded double-layer geometry. The single-cover layer and double-layer surface-wave modes' characteristic equations are examined and their cutoff conditions, along with safe conditions avoiding longitudinal-section magnetic (LSM) modes are given. The scattered field components and the TEM-wave reflection coefficient are given analytically in the form of Sommerfeld-type integrals. A thin layers approximation and a numerical integration scheme were adopted for the evaluation of the reflection coefficient. Its expression can be directly used for the analysis of wide microstrip lines and patch antennas printed in a substrate/superstrate geometry. The whole analysis gives a clear physical insight into the problem. Furthermore, a twofold theoretical verification was adopted by either forcing the absence of the superstrate or considering both layers to be isotropic. Numerical parametric investigations show the effects of either the presence of the superstrate or both layers' dielectric anisotropy.**

I. Introduction

A DIELECTRIC superstrate (cover) layer is often found necessary to be included in the analysis of microstrip antennas structures. The cover layer is either intentionally used (acting as a radome) for protection from environmental hazards, or sometimes naturally formed (e.g., ice layer) due to weather conditions. It was proven in [1]–[3] that a significant increase in patch antenna gain, radiation resistance, and its efficiency can be obtained by properly choosing the superstrate parameters. For this purpose to be achieved, fairly thick layers of the order of a quarter wavelength $(\lambda_g/4)$ have been considered. Moreover, it was proven that optimum efficiency could be achieved by a reduction, or even an elimination of surface waves. On the other hand, it is stated in [4] that when considering relatively thin layers, an increase in the superstrate layer thickness results in an efficiency reduction. It is also pointed out that the presence of the superstrate increases the edge conductance and, thus, the radiated power along with the surface-wave power are also increased. Thus, from [4] it can be concluded that unless the thickness of the two layers is taken for the resonance condition specified in [1]–[3], the superstrate should not be too thick.

Manuscript received June 3, 1996; revised January 24, 1997.

G. A. Kyriacou is with the Department of Electrical and Computer Engineering, Demokritos University of Thrace, GR-67100 Xanthi, Greece.

J. N. Sahalos is with the Department of Physics, Aristotle University of Thessaloniki, GR-54006 Thessaloniki, Greece.

Publisher Item Identifier S 0018-9480(97)02912-8.

Both layers in the above-mentioned investigations are assumed to be isotropic. A lot of dielectric materials exhibit a dielectric anisotropy, especially of the uniaxial type. This is either an inherent property of the material as in uniaxial crystalline substrates (e.g., sapphire, quartz, and magnesium fluoride) or an artificially acquired property during the manufacturing process (e.g., ceramic impregnated Teflon, like Epsilam-10). In addition, the inclusion of an also uniaxial superstrate offers more degrees of freedom in the printed circuits and antenna design toward the improvement of their performance. For this purpose, an extensive investigation of the substrate/superstrate anisotropy effects should be carried out. It is exactly toward this aim that the authors are currently working, with some preliminary results presented in [5], while an in-depth examination is to be presented in this paper.

The single-layer (substrate) uniaxial anisotropy has been the subject of the authors' previous works [6], [7]. A double-layer structure, where an uniaxial superstrate is added is analyzed in this paper. An analytic approach based on the Wiener–Hopf technique in conjunction with a space-domain Fourier spectrum is employed. This results in closed-form expressions in terms of Sommerfeld-type integrals for the scattered electromagnetic-field components, which gives a clearer physical insight compared to numerical techniques. First, the canonical problem of a TEM wave obliquely incident upon the infinitely extended edge, defined by a truncated plane conductor lying at the interface of the two uniaxial dielectric slabs is addressed. The whole scattering phenomenon near the edge, namely radiated fields, surface waves excitation, and reflected fields, is taken into account and a TEM-wave reflection coefficient (Γ_{TEM}) is established. For the case of electrically thin layers, an approximation of the integrals involved in Γ_{TEM} is carried out, resulting in an algebraic closed-form expression for Γ_{TEM}. While for electrically thick layers, a numerical integration scheme is employed for the evaluation of the integrals involved in Γ_{TEM}.

Furthermore, the established Γ_{TEM} can be used for the study of wide microstrip lines as well as rectangular and some triangular patch antennas. According to [9], [13], [15], the scattering-reflection phenomenon can be reasonably assumed to be localized for the wide microstrip lines and the most frequently encountered patch antennas in practice. Namely, their open edges can be assumed electrically isolated. Thus, the two-dimensional (2-D) reflection coefficient established herein can be used within the geometrical optics technique, e.g., [14], [15], for the study of these practical structures.

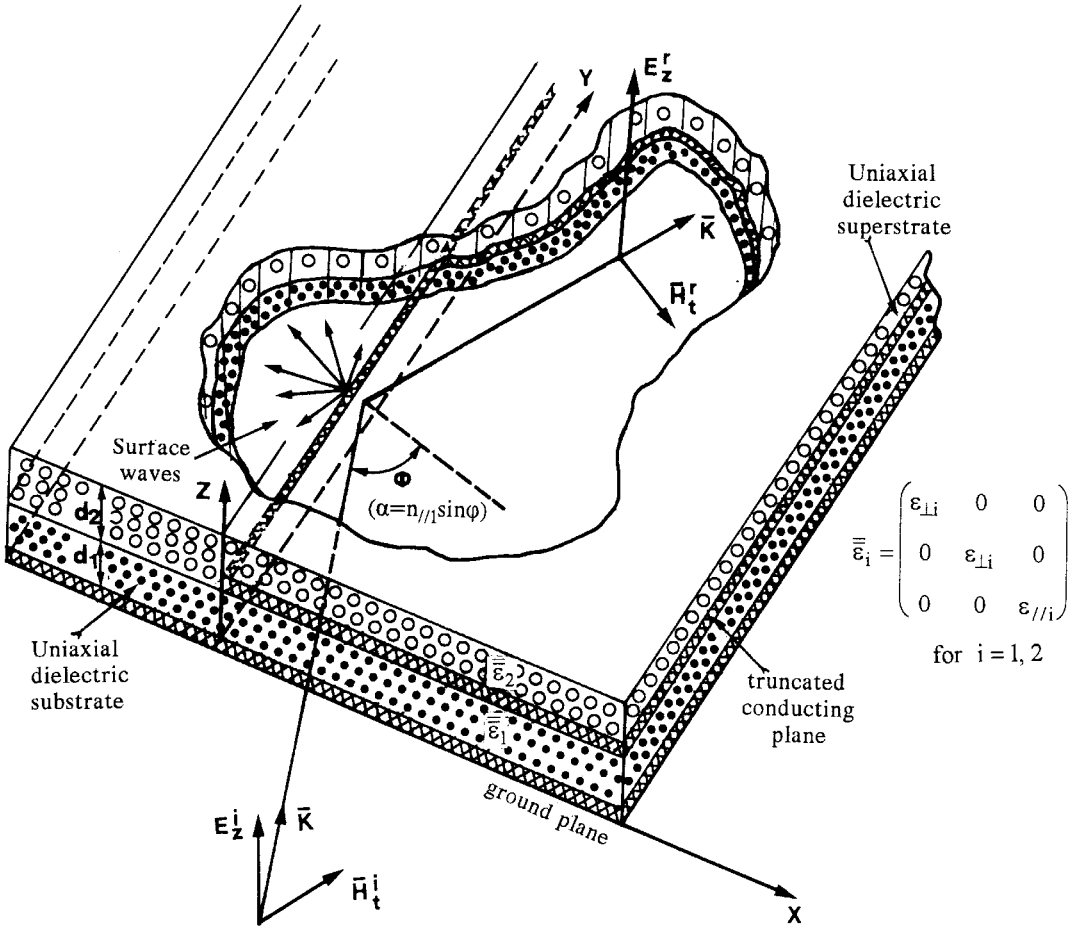

Fig. 1. An obliquely incident TEM wave at the edge of a semi-infinite plate conductor, in a uniaxial anisotropic substrate/superstrate configuration.

II. Formulation

An infinitely extended grounded double-layer dielectric structure is considered, where a semi-infinite plate conductor is located at their interface, as shown in Fig. 1. The relative magnetic permeabilities of the two slabs are symbolized as μ_{ri} $(i = 1, 2)$, while their dielectric permittivities are assumed uniaxially anisotropic with their optical axis vertically aligned along the z-axis, described by tensors of the form

$$\bar{\bar{\varepsilon}}_{ri} = \begin{pmatrix} \varepsilon_{xi} & 0 & 0 \\ 0 & \varepsilon_{yi} & 0 \\ 0 & 0 & \varepsilon_{zi} \end{pmatrix} = \begin{pmatrix} \varepsilon_{\perp i} & 0 & 0 \\ 0 & \varepsilon_{\perp i} & 0 \\ 0 & 0 & \varepsilon_{//i} \end{pmatrix}, \qquad \text{for } i = 1, 2. \tag{1a}$$

The *optical axis* is a term widely used for the uniaxial media. Further details can be found in [16]. The corresponding refractive indices are then

$$n_{\perp i} = \sqrt{\varepsilon_{\perp i}\mu_{ri}}$$

and

$$n_{//i} = \sqrt{\varepsilon_{//i}\mu_{ri}}. \tag{1b}$$

A Wiener–Hopf solution of the canonical problem of a vertically polarized TEM propagating in layer one and obliquely incident (at an angle ϕ) upon the opening defined by the truncated conductor, is to be tried first. A TEM-wave reflection coefficient will then be defined, followed by parametric investigations for the edge admittance and its applications in the study of microstrip structures. The incident wave, propagating in region one, can be expressed as

$$E_z^i = e^{-jk_0(-\xi x+\alpha y)}$$

and

$$\overline{H}_t^i = \frac{1}{\mu_{r1}\zeta_0}(\alpha\hat{x} + \xi\hat{y})e^{-jk_0(-\xi x+\alpha y)} \tag{2}$$

where $\alpha = n_{//1}\sin\phi$ and $\xi = n_{//1}\cos\phi = \sqrt{n_{//1}^2 - \alpha^2}$ are the propagation constants in the y- and x-direction, respectively, and $\zeta_0 = 120\pi\ \Omega$ is the free-space intrinsic impedance.

The scattered field components are determined by the help of a space-domain Fourier transform in conjunction with the *hybrid-mode* analysis technique. Time harmonic fields of the form $e^{j\omega t}$ and a λ-space spectrum Fourier transform pair in the x-direction are considered as

$$\tilde{f}(\lambda) = \frac{k_0}{2\pi}\left\{\int_{-\infty}^{0} + \int_{0}^{\infty}\right\} f(x)e^{jk_0\lambda x}\,dx = \tilde{f}_-(\lambda) + \tilde{f}_+(\lambda)$$

and

$$f(x) = \int_{-\infty}^{\infty} \tilde{f}(\lambda)e^{-jk_0\lambda x}\,d\lambda. \tag{3}$$

$\tilde{f}_+(\lambda)$ and $\tilde{f}_-(\lambda)$, defined as positive and negative functions, are analytic in the upper- and lower-complex λ-planes, respectively. Since there is not any discontinuity in the y-direction, the scattered field will also be propagating along the y-axis as $e^{-jk_0\alpha y}$, like the incident field. (The dependencies $e^{j\omega t}$ and $e^{-jk_0\alpha y}$ apply for all the field quantities, but they are omitted for convenience throughout this paper.) In this manner, Maxwell's equations can be simplified with the resulting substitutions: $\partial/\partial t \rightarrow j\omega$, $\partial/\partial y \rightarrow -jk_0\alpha$, and $\partial/\partial x \rightarrow -jk_0\lambda$.

Furthermore, according to the hybrid-mode analysis, the scattered field can be given by a superposition of longitudinal-section electric (LSE) modes or transverse to the z-axis TE_z with $E_z = 0$ and the corresponding magnetic modes longitudinal-section magnetic (LSM) or TM_z with $H_z = 0$ as

$$\tilde{\overline{E}}^s_{ti} = \frac{1}{\alpha^2+\lambda^2}\left\{\zeta_0\mu_{ri}(\alpha\hat{x}+\lambda\hat{y})\tilde{H}^s_{zi} - \frac{j}{k_0}\left(\frac{\varepsilon_{//i}}{\varepsilon_{\perp i}}\right)(\lambda\hat{x}-\alpha\hat{y})\frac{\partial\tilde{E}^s_{zi}}{\partial z}\right\}$$

and

$$\tilde{\overline{H}}^s_{ti} = \frac{1}{\alpha^2+\lambda^2}\left\{-\frac{\varepsilon_{//i}}{\zeta_0}(\alpha\hat{x}+\lambda\hat{y})\tilde{E}^s_{zi} - \frac{j}{k_0}(\lambda\hat{x}-\alpha\hat{y})\frac{\partial\tilde{H}^s_{zi}}{\partial z}\right\}. \quad (4)$$

The subscript i denotes the three regions ($i = 0$ for the air and $i = 1, 2$ within the two dielectric slabs). The field z-components defined as $\tilde{H}^s_{zi} = \tilde{H}^{s,\mathrm{LSE}}_{zi}$ and $\tilde{E}^s_{zi} = \tilde{E}^{s,\mathrm{LSE}}_{zi}$ satisfy the following wave equations:

$$\frac{\partial^2\tilde{H}^s_{zi}}{\partial z^2} - k_0^2[u^{(i)}_{n1}]^2\tilde{H}^s_{zi} = 0$$

and

$$\frac{\partial^2\tilde{E}^s_{zi}}{\partial z^2} - k_0^2[u^{(i)}_{n2}]^2\tilde{E}^s_{zi} = 0 \quad (5)$$

where

$$u^{(i)}_{n1} = \sqrt{\alpha^2+\lambda^2-n^2_{\perp i}}$$

and

$$u^{(i)}_{n2} = \frac{n_{\perp i}}{n_{//i}}\sqrt{\alpha^2+\lambda^2-n^2_{//i}}.$$

The solutions of wave equations (5) for the air region are

$$\left.\begin{aligned}\tilde{E}^s_{z0} &= E_0 e^{-k_0u_0z}\\ \tilde{H}^s_{z0} &= H_0 e^{-k_0u_0z}\end{aligned}\right\}, \qquad \text{for } z \geq d_{12} = d_1 + d_2 \quad (6)$$

where $u_0 = \sqrt{\alpha^2+\lambda^2-1}$ and the real part of all u-functions must be positive $\mathrm{Re}\{u_0\}$, $\mathrm{Re}\{u^{(i)}_{n1}\}$, $\mathrm{Re}\{u^{(i)}_{n2}\} \geq 0$.

The corresponding solutions in the two dielectric slab regions $i = 1, 2$ are

$$\begin{aligned}\tilde{E}^s_{zi} &= E^{(i)}_{ns}\sinh[k_0u^{(i)}_{n2}z] + E^{(i)}_{nc}\cosh[k_0u^{(i)}_{n2}z]\\ \tilde{H}^s_{zi} &= H^{(i)}_{ns}\sinh[k_0u^{(i)}_{n1}z] + H^{(i)}_{nc}\cosh[k_0u^{(i)}_{n1}z].\end{aligned} \quad (7)$$

Region one is $0 \leq z \leq d_1$ and region two is $d_1 \leq z \leq d_{12}$.

The total tangential electric field must be continuous at the interfaces $z = 0$, d_1, and d_{12}. Since the incident tangential electric field is zero then the continuity must be satisfied by the scattered one. Using (4), the latter requirement imposes the continuity of the quantities $\mu_{ri}\tilde{H}^s_{zi}$ and $(\varepsilon_{//i}/\varepsilon_{\perp i})(\partial\tilde{E}^s_{zi}/\partial z)$. These conditions yield the following.

1) On the infinite ground plane (zero tangential electric field) at $z = 0$:

$$\begin{aligned}E^{(1)}_{ns} &= 0\\ H^{(1)}_{nc} &= 0.\end{aligned} \quad (8)$$

2) On the interface $z = d_1$ (incident field $\overline{E}^i_t = 0$):

$$\begin{aligned}&\frac{\varepsilon_{//1}}{\varepsilon_{\perp 1}}u^{(1)}_{n2}E^{(1)}_{nc}\sinh[k_0u^{(1)}_{n2}d_1]\\ &\quad= \frac{\varepsilon_{//2}}{\varepsilon_{\perp 2}}u^{(2)}_{n2}\{E^{(2)}_{ns}\cosh[k_0u^{(2)}_{n2}d_1] + E^{(2)}_{nc}\sinh[k_0u^{(2)}_{n2}d_1]\}\end{aligned} \quad (9a)$$

$$\begin{aligned}&\mu_{r1}H^{(1)}_{ns}\sinh[k_0u^{(1)}_{n1}d_1]\\ &\quad= \mu_{r2}\{H^{(2)}_{ns}\sinh[k_0u^{(2)}_{n1}d_1] + H^{(2)}_{nc}\cosh[k_0u^{(2)}_{n1}d_1]\}.\end{aligned} \quad (9b)$$

3) On the interface $z = d_1 + d_2 = d_{12}$:

$$\begin{aligned}&\frac{\varepsilon_{//2}}{\varepsilon_{\perp 2}}u^{(2)}_{n2}\{E^{(2)}_{ns}\cosh[k_0u^{(2)}_{n2}d_{12}] + E^{(2)}_{nc}\sinh[k_0u^{(2)}_{n2}d_{12}]\}\\ &\quad= -u_0E_0e^{-k_0u_0d_{12}}\end{aligned} \quad (10a)$$

$$\begin{aligned}&\mu_{r2}\{H^{(2)}_{ns}\sinh[k_0u^{(2)}_{n1}d_{12}] + H^{(2)}_{nc}\cosh[k_0u^{(2)}_{n1}d_{12}]\}\\ &\quad= H_0e^{-k_0u_0d_{12}}.\end{aligned} \quad (10b)$$

Also, the tangential magnetic field must be continuous on the air–dielectric interface. Thus, (4) imposes the continuity of $\varepsilon_{//i}\tilde{E}^s_{zi}$ and $\partial\tilde{H}^s_{zi}/\partial z$, which at $z = d_{12}$ gives

$$\begin{aligned}&\varepsilon_{//2}\{E^{(2)}_{ns}\sinh[k_0u^{(2)}_{n2}d_{12}] + E^{(2)}_{nc}\cosh[k_0u^{(2)}_{n2}d_{12}]\}\\ &\quad= E_0e^{-k_0u_0d_{12}}\end{aligned} \quad (11a)$$

$$\begin{aligned}&u^{(2)}_{n1}\{H^{(2)}_{ns}\cosh[k_0u^{(2)}_{n1}d_{12}] + H^{(2)}_{nc}\sinh[k_0u^{(2)}_{n1}d_{12}]\}\\ &\quad= -u_0H_0e^{-k_0u_0d_{12}}.\end{aligned} \quad (11b)$$

A Wiener–Hopf equation for the scattered z-component electric field can be found by applying the boundary conditions for the total electric flux density vector $D_{zt} = \varepsilon_0\overline{\overline{\varepsilon}}E_{zt}$ at the interface $z = d_1$. The normal scattered flux D^s_z is continuous at the interface between dielectrics -1 and -2 (for $x < 0$) and discontinuous on the truncated conductor (for $x > 0$) by the amount of the induced surface charge density $\rho^s(x)$. The authors follow the procedure given in [1] and recall that the quantity $-\varepsilon_0\varepsilon_{//1}E^i_z(x, z = d_1^-)$ for $x < 0$ can be treated as a fictitious surface-charge density $\rho^i(x)$. This is the charge density that would be induced at the interface ($z = d_1$, $x < 0$) if the plate conductor was not truncated. This results from an equivalent situation where the incident field is assumed to be confined within the first layer; namely the incident field, is assumed to be zero above the dielectric–air interface $z = d_1$. Under this approach, and in order for the boundary condition

of the normal flux D_z^i to be valid, a fictitious charge density $\rho_{(x)}^i$ must be included at ($z = d_1$, $x < 0$) as

$$D_z^i(x<0,\, z=d_1^+) - D_z^i(x<0,\, z=d_1^-) = \rho^i(x<0)$$

or

$$0 - \varepsilon_0\varepsilon_{//1}E_z^i(x<0,\ z=d_1^-) = \rho^i(x<0).$$

Taking into account the boundary conditions for the scattered component D_z^s at ($z = d_1$, $x > 0$) and for both D_z^s and the incident component D_z^i at ($z = d_1$, $x < 0$) one finally gets

$$\varepsilon_{//2}\tilde{E}_z^{s(2)}(\lambda,\, z=d_1^+) = \varepsilon_{//1}\tilde{E}_z^{s(1)}(\lambda,\, z=d_1^-) - \frac{\tilde{\rho}_-^i(\lambda)}{\varepsilon_0} + \frac{\tilde{\rho}_+^s(\lambda)}{\varepsilon_0} \tag{12}$$

where $\tilde{\rho}_-^i(\lambda)$ and $\tilde{\rho}_+^s(\lambda)$ are the Fourier transforms of $\rho^i(x)$ and $\rho^s(x)$, and are analytic in the lower and upper complex-λ half planes.

The Fourier integral of the known incident electric field E_z^i ($x < 0$, $z = d_1^-$) can be evaluated analytically yielding the $\tilde{\rho}_-^i(\lambda)$ in the form

$$\tilde{\rho}_-^i(\lambda) = j\,\frac{\varepsilon_0\varepsilon_{//1}}{2\pi}\,\frac{e^{-jk_0\alpha y}}{\lambda + \sqrt{n_{//1}^2 - \alpha^2}}. \tag{13}$$

The total charge induced on the truncated conductor can also be expressed by the divergence of the total tangential flux density D_{zt}^s. For this purpose, the authors define a function $\tilde{F}_-(\lambda)$ analytic in the lower complex-λ half plane as

$$\begin{aligned}\tilde{F}_-(\lambda) &= \frac{1}{2\pi}\int_{-\infty}^{0} \overline{\nabla}_t \cdot \overline{E}_{t1}^s(x,\, z=d_1)e^{jk_0\lambda x}\,dx \\ &= j[-\lambda\tilde{E}_{x1-}^s + \alpha\tilde{E}_{y1-}^s]_{z=d_1}.\end{aligned} \tag{14}$$

The unknowns $E_{nc}^{(1)}$, $E_{ns}^{(2)}$, and $E_{nc}^{(2)}$ can be expressed as a function of $\tilde{F}_-(\lambda)$ through (9a), (10a), (11a), and (14). The resulting expressions are as follows:

$$E_{nc}^{(1)} = -\frac{\varepsilon_{\perp 1}}{\varepsilon_{//1}}\,\frac{\tilde{F}_-(\lambda)}{u_{n2}^{(1)}\,\sinh[k_0u_{n2}^{(1)}d_1]}$$

$$E_{ns}^{(2)} = -\frac{\varepsilon_{\perp 2}}{\varepsilon_{//2}}\,\frac{\tilde{F}_-(\lambda)}{u_{n2}^{(2)}\{\cosh[k_0u_{n2}^{(2)}d_1] - f(\lambda)\,\sinh[k_0u_{n2}^{(2)}d_1]\}}$$

$$E_{nc}^{(2)} = -\frac{\varepsilon_{\perp 2}}{\varepsilon_{//2}}\,\frac{\tilde{F}_-(\lambda)}{u_{n2}^{(2)}\left\{\sinh[k_0u_{n2}^{(2)}d_1] - \dfrac{1}{f(\lambda)}\,\cosh[k_0u_{n2}^{(2)}d_1]\right\}}$$

where

$$f(\lambda) = \frac{u_{n2}^{(2)} + \varepsilon_{\perp 2}\,\tanh[k_0u_{n2}^{(2)}d_{12}]}{\varepsilon_{\perp 2}u_0 + u_{n2}^{(2)}\,\tanh[k_0u_{n2}^{(2)}d_{12}]}.$$

Substituting these into (12), and after some algebraic manipulations, one gets the following Wiener–Hopf equation:

$$\tilde{F}_-(\lambda) = Q_e(\lambda)\,\frac{\tilde{\rho}_+^s(\lambda) - \tilde{\rho}_-^i(\lambda)}{\varepsilon_0} \tag{15}$$

as shown in (16a) and (16b) at the bottom of the page. The characteristic equations of the excited LSE modes are introduced in (15) and (16) as will be explained in the following section.

In the same manner as above, a Wiener–Hopf equation for the magnetic field can be found by imposing the boundary conditions for the total magnetic field on the truncated conductor and at the interface of the two dielectrics. The tangential magnetic field must be continuous at the interface $z = d_1$ between the two dielectrics (for $x < 0$), while it must be discontinuous by the amount of the total induced surface current density $\overline{J}_t$ on the truncated conductor (for $x > 0$). This boundary condition in its usual form can be written as $\overline{H}_2 - \overline{H}_1 = -\hat{z} \times \overline{J}_t$. In order to reduce this vector form into a scalar one, one can take its divergence as $\overline{\nabla}_t \cdot (\overline{H}_2 - \overline{H}_1) = -\overline{\nabla}_t \cdot (\hat{z} \times \overline{J}_t)$, where the operator $\overline{\nabla}$ is reduced to $\overline{\nabla}t$ since only the tangential components are involved. For convenience, let $H_z' = \overline{\nabla} \bullet \overline{H}_t$. In this manner this boundary condition gives the following relation in the Fourier domain:

$$\tilde{H}_{z2}^{s'}(\lambda,\, z=d_1^+) - \tilde{H}_{z1}^{s'}(\lambda,\, z=d_1^-) = \tilde{j}_+(\lambda) \tag{17}$$

where $\tilde{H}_{zi}^{s'}$ and $\tilde{j}_+$ are the Fourier transforms of the quantities $H_{zi}^{s'}$ and $-\overline{\nabla}_t \cdot [\hat{z} \times \overline{J}_t(x)]$, which is

$$H_{zi}^{s'}(x,\, z) = \overline{\nabla}_t \cdot \overline{H}_{ti}^s$$

and

$$\tilde{H}_{zi}^{s'} = jk_0(\lambda\tilde{H}_{xi}^s - \tilde{H}_{yi}^s). \tag{18}$$

It can easily be proved from (2) that for the incident magnetic field $\overline{\nabla}_t \cdot \overline{H}_t^i = 0$. This means that the surface current density involved in (17) is exclusively coming from the scattered magnetic field, thus $\overline{J}_t(x) = \overline{J}_t^s(x)$ or $\tilde{j}_+(\lambda) = j_+^s(\lambda)$.

In order to establish another relation between the unknowns $H_{ns}^{(1)}$, $H_{ns}^{(2)}$, and $H_{nc}^{(2)}$, beside that of (17), a function $\tilde{G}_-(\lambda)$ analytic in the lower-λ half plane is defined from the rotation of the tangential electric field on the truncated conductor as

$$\begin{aligned}\tilde{G}_-(\lambda) &= \frac{1}{2\pi}\int_{-\infty}^{0} \hat{z} \cdot \overline{\nabla}_t \times \overline{E}_t^s(x,\, z=d_1)e^{jk_0\lambda x}\,dx \\ &= j[\alpha\tilde{E}_{x-}^s + \lambda\tilde{E}_{y-}^s]_{z=d_1}.\end{aligned} \tag{19}$$

---

where

$$Q_e(\lambda) = \frac{u_{n2}^{(1)}u_{n2}^{(2)}\,\tanh[k_0u_{n2}^{(1)}d_1]}{D_{\mathrm{LSE}}} \tag{16a}$$

and

$$D_{\mathrm{LSE}} = \varepsilon_{\perp 1}u_{n2}^{(2)} + \frac{\{u_{n2}^{(2)} + \varepsilon_{\perp 2}u_0\,\tanh[k_0u_{n2}^{(2)}d_2]\}\varepsilon_{\perp 2}u_{n2}^{(1)}\,\tanh[k_0u_{n2}^{(1)}d_1]}{\varepsilon_{\perp 2}u_0 + u_{n2}^{(2)}\,\tanh[k_0u_{n2}^{(2)}d_2]} \tag{16b}$$

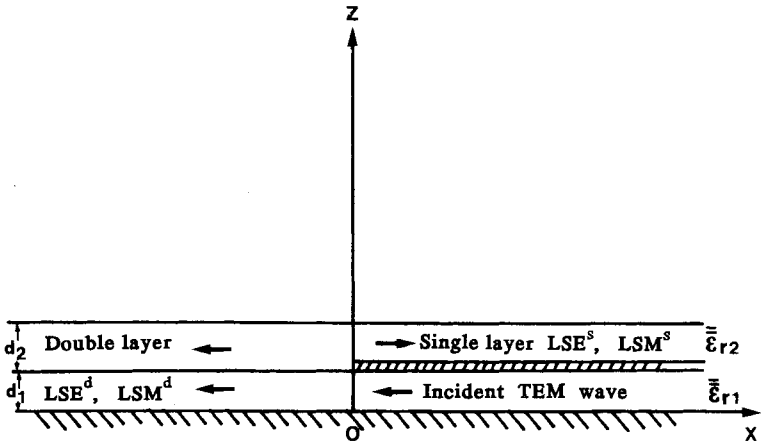

Fig. 2. Single- (upper) and double-layer surface waves propagating in the $x > 0$ and $x < 0$ directions, respectively.

The unknowns $H_{ns}^{(1)}$, $H_{ns}^{(2)}$, and $H_{nc}^{(2)}$ can be expressed in terms of $\tilde{G}_-(\lambda)$ through (9b), (10b), and (11b) as

$$H_{ns}^{(1)} = j\,\frac{\tilde{G}_-(\lambda)}{\zeta_0\mu_{r1}\,\sinh[k_0u_{n1}^{(1)}d_1]}$$

$$H_{ns}^{(2)} = j\,\frac{\tilde{G}_-(\lambda)}{\zeta_0\mu_{r2}\{\sinh[k_0u_{n1}^{(2)}d_1] - g(\lambda)\,\cosh[k_0u_{n1}^{(2)}d_1]\}}$$

$$H_{nc}^{(2)} = j\,\frac{\tilde{G}_-(\lambda)}{\zeta_0\mu_{r2}\left\{\cosh[k_0u_{n1}^{(2)}d_1] - \dfrac{1}{g(\lambda)}\,\sinh[k_0u_{n1}^{(2)}d_1]\right\}}$$

where

$$g(\lambda) = \frac{u_{n1}^{(2)} + \mu_{r2}u_0\,\tanh[k_0u_{n1}^{(2)}d_{12}]}{\mu_{r2}u_0 + u_{n1}^{(2)}\,\tanh[k_0u_{n1}^{(2)}d_{12}]}.$$

Substituting the above relations in (17) and using the expressions (7), after a relatively long algebraic manipulation, one gets the following Wiener–Hopf equation:

$$\tilde{G}_-(\lambda) = \frac{1}{j\omega\varepsilon_0}\,Q_m(\lambda)\tilde{j}_+(\lambda) \tag{20}$$

where

$$Q_m(\lambda) = \frac{\mu_{r1}\mu_{r2}}{D_{\mathrm{LSM}}} \tag{21a}$$

and

$$D_{\mathrm{LSM}} = \mu_{r2}u_{n1}^{(1)}\,\coth[k_0u_{n1}^{(1)}d_1] + \frac{\mu_{r1}u_{n1}^{(2)}\{u_{n1}^{(2)} + \mu_{r2}u_0\,\coth[k_0u_{n1}^{(2)}d_2]\}}{\mu_{r2}u_0 + u_{n1}^{(2)}\,\coth[k_0u_{n1}^{(2)}d_2]}. \tag{21b}$$

As is expected, the excited LSM modes characteristic equations are introduced in (20) and (21).

III. LSE, LSM Surface Modes Characteristic Equations

Two groups of surface waves are supported by the structure of Fig. 1, which are clearly shown in Fig. 2. The first group is supported by the "grounded" (over the truncated conductor) superstrate layer in the area $x > 0$. The second group is supported by the grounded double layer (over the infinite conductor) in the area $x < 0$. Both of these surface waves are excited by the TEM incident wave at the edge $x = 0$. The first group propagates in the cover layer toward $x > 0$, while the second group propagates in both layers toward $x < 0$.

The characteristic equations for the modes of the upper grounded layer can be found by considering the truncated conductor at $z = d_1$ to be extended infinitely ($-\infty < x < \infty$). For such a situation the tangential electric field must vanish on the infinite conductor. This yields

$$\tilde{\bar{E}}_{t2}^{s}\Big|_{z=d_1} = 0$$

or

$$\frac{\partial\tilde{E}_{z2}^{s}}{\partial z}\Big|_{z=d_1} = 0$$

and

$$\tilde{H}_{z2}^{s}\Big|_{z=d_1} = 0$$

or explicitly

$$\left.\begin{aligned} E_{ns}^{(2)}u_{n2}^{(2)}\,\cosh[k_0u_{n2}^{(2)}d_1] + E_{nc}^{(2)}u_{n2}^{(2)}\,\sinh[k_0u_{n2}^{(2)}d_1] = 0 \\ H_{ns}^{(2)}\,\sinh[k_0u_{n1}^{(2)}d_1] + H_{nc}^{(2)}\,\cosh[k_0u_{n1}^{(2)}d_1] = 0 \end{aligned}\right\}. \tag{22}$$

Equation (22), along with the boundary conditions at the interface $z = d_{12}$ given by (10) and (11), leads to the following two characteristic equations:

Grounded upper layer LSE modes:

$$\left.\begin{aligned} &u_{n2}^{(2)}\,\tanh[k_0u_{n2}^{(2)}d_2] = -\varepsilon_{\perp 2}u_0 \\ &\text{or} \\ &\frac{n_{\perp 2}}{n_{//2}}\sqrt{n_{//2}^2 - \alpha_{pe}^2}\,\tan\left(k_0d_2\,\frac{n_{\perp 2}}{n_{//2}}\sqrt{n_{//2}^2 - \alpha_{pe}^2}\right) \\ &\quad = \varepsilon_{\perp 2}\sqrt{\alpha_{pe}^2 - 1} \end{aligned}\right\} \tag{23}$$

Grounded upper layer LSM modes:

$$\left.\begin{aligned} & u_{n1}^{(2)} \coth[k_0 u_{n1}^{(2)} d_2] = -\mu_{r2} u_0 \\ & \sqrt{n_{\perp 2}^2 - \alpha_{pm}^2} \cot\left(k_0 d_2 \sqrt{n_{\perp 2}^2 - \alpha_{pm}^2}\right) \\ & \quad = -\mu_{r2} \sqrt{\alpha_{pm}^2 - 1} \end{aligned}\right\} \quad (24)$$

where α_{pe} and α_{pm} ($\rightarrow \alpha^2+\lambda^2$) are the propagation constants of LSE and LSM modes, respectively, and $p = 1, 2, \cdots$ is the order of the mode.

The characteristic equations for the grounded double layer can be obtained by considering the absence of the truncated conductor at $z = d_1$. In such a case there is not any surface current flowing along the interface $z = d_1$ and the tangential magnetic field must be continuous across it. This gives

$$\tilde{\overline{H}}_{t1}^{s}\Big|_{z=d_1^-} = \tilde{\overline{H}}_{t2}^{s}\Big|_{z=d_1^+}$$

or

$$\varepsilon_{//1} \tilde{E}_{z1}^{s}\Big|_{z=d_1^-} = \varepsilon_{//2} \tilde{E}_{z2}^{s}\Big|_{z=d_1^+}$$

and

$$\frac{\partial \tilde{H}_{z1}^{s}}{\partial z}\Big|_{z=d_1^-} = \frac{\partial \tilde{H}_{z2}^{s}}{\partial z}\Big|_{z=d_1^+}$$

or explicitly

$$\left.\begin{aligned} & \varepsilon_{//1} E_{nc}^{(1)} \cosh[k_0 u_{n2}^{(1)} d_1] \\ & \quad = \varepsilon_{//2}\{E_{ns}^{(2)} \sinh[k_0 u_{n2}^{(2)} d_1] + E_{nc}^{(2)} \cosh[k_0 u_{n2}^{(2)} d_1]\} \\ & u_{n1}^{(1)} H_{ns}^{(1)} \cosh[k_0 u_{n1}^{(1)} d_1] \\ & \quad = u_{n1}^{(2)}\{H_{ns}^{(2)} \cosh[k_0 u_{n1}^{(2)} d_1] + H_{nc}^{(2)} \sinh[k_0 u_{n1}^{(2)} d_1]\} \end{aligned}\right\}. \quad (25)$$

The rest of the boundary conditions (except for the truncated conductor) are valid exactly as in the previous section. So, the combination of expressions (8)–(11) with (25) results in the following characteristic equations:

Grounded double layer, LSE modes:

$$D_{\mathrm{LSE}} = 0 \quad (26)$$

with D_{LSE}, given by (16b).

Grounded double layer, LSM modes:

$$D_{\mathrm{LSM}} = 0 \quad (27)$$

with D_{LSM} given by (21b).

Inspecting the two Wiener–Hopf equations [(15) and (20)], one can see that the double-layer surface waves characteristic equations are introduced inside them as denominators: LSE modes in the electric field and LSM modes in the magnetic field. The cover-layer surface-waves characteristic (23) and (24), are in turn, introduced inside D_{LSE} and D_{LSM}, respectively.

IV. Solution of the Wiener–Hopf Equations

The two kernels Q_e and Q_m involved in the Wiener–Hopf equations are first factored into a product of a positive and negative function: $Q_e = Q_{e+} \cdot Q_{e-}$ and $Q_m = Q_{m+} \cdot Q_{m-}$, according to [8]. Similarly following [7] and [13], one finally obtains the following solutions:

$$\begin{aligned} \tilde{F}_-(\lambda) = & -j \frac{k_0 d_1}{\pi} \sqrt{n_{//1}^2 - \alpha^2} \\ & \cdot \left\{ \frac{\lambda + j\alpha \tanh \Delta}{\sqrt{n_{//1}^2 - \alpha^2} - j\alpha \tanh \Delta} \right\} \\ & \cdot e^{-j\left[f_e(-\lambda) + f_e\left(-\sqrt{n_{//1}^2 - \alpha^2}\right)\right]/2} \end{aligned} \quad (28)$$

and

$$\begin{aligned} \tilde{G}_-(\lambda) = & -j \frac{k_0 d_1}{\pi} \sqrt{n_{//1}^2 - \alpha^2} \\ & \cdot \frac{\alpha e^{-j\left[f_e\left(-\sqrt{n_{//1}^2 - \alpha^2}\right) + f_m(-\lambda)\right]/2}}{\sqrt{n_{//1}^2 - \alpha^2} \cosh \Delta - j\alpha \sinh \Delta} \end{aligned} \quad (29)$$

where (see (30) at the bottom of the page), and

$$\begin{aligned} \Delta(\alpha) = & \frac{\alpha}{\pi} \int_0^\infty \ell n\left\{ \frac{\varepsilon_{\perp 1} u_{n2}^{(2)} \tanh[k_0 u_{n2}^{(1)} d_1] D_{\mathrm{LSM}}}{\mu_{r2} u_{n2}^{(1)} D_{\mathrm{LSE}}} \right\} \\ & \cdot \frac{d\lambda}{\lambda^2 + \alpha^2}. \end{aligned} \quad (31)$$

$$\left.\begin{aligned} f_e(\lambda) = & j\ell n\left\{ \frac{\varepsilon_{\perp 1}}{k_0 d_1} \frac{\dfrac{n_{//1}}{n_{\perp 1}} \dfrac{n_{\perp 2}}{n_{//2}}}{\left\{\varepsilon_{\perp 1}\left(\dfrac{n_{\perp 2}}{n_{//2}}\right) + \varepsilon_{\perp 2}\left(\dfrac{n_{\perp 1}}{n_{//1}}\right)\right\}\left(\sqrt{\alpha^2 - 1} - j\lambda\right)} \right\} + \frac{2\lambda}{\pi} \int_0^\infty \ell n\{q_e(w)\} \frac{dw}{w^2 - \lambda^2} \\ f_m(\lambda) = & j\ell n\left\{ \frac{\mu_{r2}}{k_0 d_1 (\mu_{r1} + \mu_{r2})\left(\sqrt{\alpha^2 - 1} - j\lambda\right)} \right\} + \frac{2\lambda}{\pi} \int_0^\infty \ell n\{q_m(w)\} \frac{dw}{w^2 - \lambda^2} \\ q_e(\lambda) = & \frac{\varepsilon_{\perp 1}\left(\dfrac{n_{\perp 2}}{n_{//2}}\right) + \varepsilon_{\perp 2}\left(\dfrac{n_{\perp 1}}{n_{//1}}\right)}{\dfrac{n_{//1}}{n_{\perp 1}} \dfrac{n_{\perp 2}}{n_{//2}}} \frac{u_0 u_{n2}^{(2)} \tanh[k_0 u_{n2}^{(1)} d_1]}{u_{n2}^{(1)} D_{\mathrm{LSE}}} \\ q_m(\lambda) = & \frac{(\mu_{r1} + \mu_{r2}) u_0}{D_{\mathrm{LSM}}} \end{aligned}\right\} \quad (30)$$

Since all the λ-functions (unknown at the beginning) involved in the expressions of the electromagnetic field are already given in terms of either $\tilde{F}_-(\lambda)$ or $\tilde{G}_-(\lambda)$, then (28)–(31) can be used to obtain the desired field components. The difficulty to be faced now is that the obtained expressions are in the Fourier domain and an inverse Fourier transform is required in order to get the field components in the real domain. This task presents major difficulties in the general case, since the functions $\tilde{F}_-(\lambda)$ and $\tilde{G}_-(\lambda)$, and in turn the field spectral components, are already in the form of Sommerfeld-type integrals, as shown above.

Fortunately, there is a number of cases with practical interest, like the reflection or the transmission coefficient of the TEM wave where the inverse Fourier integral can be approximated by its residue (or Cauchy principal value) contribution.

At this point, as well as at the end of some major steps within the present analysis, a twofold theoretical verification is adopted. First, by considering the absence of the superstrate (zero thickness and unit dielectric constant) all expressions are exactly reduced to those of the authors' previous work [5], [7], and are carried out by considering a uniaxial substrate, as well as one without a superstrate. Second, by letting the two dielectric layers become isotropic (namely $\varepsilon_{//1} = \varepsilon_{\perp 1} = \varepsilon_{r1}$ and $\varepsilon_{\perp 2} = \varepsilon_{//2} = \varepsilon_{r2}$), and considering normal incidence ($\alpha = 0$) as in [4], the corresponding expressions appearing therein are exactly verified.

V. Reflection Coefficient

All surface waves mentioned earlier are excited near the edge $x = 0$, in the vicinity of the point where the z-polarized TEM wave is incident. In general, these two infinite series of LSE and LSM modes must be taken into account by means of their residue contributions at the poles (propagation constants) $\lambda = \pm\alpha_{pm}, \pm\alpha_{pe}$ given by the solution of (23), (24), (26), and (27). Higher order modes have large attenuation constants and vanish quickly from the edge. At an adequate distance away from the edge, only the dominant reflected z-polarized TEM wave will exist and its contribution is given by the residue at $\lambda = \sqrt{n_{//1}^2 - \alpha^2}$. This is the case for wide microstrip lines and antennas. It is quite convenient for these applications to account for the reflected TEM wave by the aid of the corresponding reflection coefficient. This is defined as the ratio of the reflected-to-incident TEM wave z-component of the electric field. The scattered z-component of the electric field within the substrate $E_{z1}^s(x)$ can be obtained by applying the inverse Fourier transform to $\tilde{E}_{z1}^s(\lambda)$ given by (7a) where the function $E_{nc}^{(1)}(\lambda)$ is taken by its expression with $\tilde{F}_-(\lambda)$. It is then

$$E_{z1}^s(x) = \int_{-\infty}^{\infty} \tilde{E}_{z1}^s(\lambda) e^{-jk_0\lambda x}\, dx = -\frac{\varepsilon_{\perp 1}}{\varepsilon_{//1}} \int_{-\infty}^{\infty} \frac{\cosh[k_0 u_{n2}^{(1)} z]\tilde{F}_-(\lambda) e^{-jk_0\lambda x}}{u_{n2}^{(1)} \sinh[k_0 u_{n2}^{(1)} d_1]}\, dx.$$

Since the interest here is in the reflected wave, which exists in the $x > 0$ area, the contour of integration is closed in the lower-λ half plane. The TEM-wave scattered field is obtained from the residue contribution of the corresponding pole at $\lambda = \sqrt{n_{//1}^2 - \alpha^2}$ [for which $u_{n2}^{(1)} = 0$]. The resulting reflection coefficient is then expressed as

$$\begin{aligned}\Gamma_{(\mathrm{TEM})}(\alpha) &= \frac{E_{z1}^s(x, y)|_{\mathrm{TEM}}}{E_z^i|_{\mathrm{TEM}}} \\ &= j\pi \frac{\tilde{F}_-\left(\lambda = \sqrt{n_{//1}^2 - \alpha^2}\right)}{k_0 d_1 \sqrt{n_{//1}^2 - \alpha^2}} \\ &= e^{jX(\alpha)}\end{aligned} \tag{32}$$

where

$$X(\alpha) = 2\tan^{-1}\left(\frac{\alpha \tanh\Delta}{\sqrt{n_{//1}^2 - \alpha^2}}\right) - f_e\left(-\sqrt{n_{//1}^2 - \alpha^2}\right). \tag{33}$$

The functions $\Delta(\alpha)$ and $f_e(\lambda)$ are given as semi-infinite integrals with respect to λ or w. For the purpose of this paper, either numerical integration or analytical approximation will be employed depending on the two layers thickness. An examination of (30) shows that the main contribution to the $f_e(\lambda)$ integral comes from the pole $w \to \lambda = \sqrt{n_{//1}^2 - \alpha^2}$. It is then more convenient for numerical integration purposes to extract this $f_e(w \to \lambda)$ contribution analytically. But, as in the usual case (small dielectric losses), this pole lies near the $\mathrm{Re}\,(w)$ axis and the integration is from 0 to ∞, thus this contribution is actually a Cauchy principal value. The resulting principal-value integral is

$$\begin{aligned}f_e\left(\lambda = -\sqrt{n_{//1}^2 - \alpha^2}\right) &= \tan^{-1}\left(\frac{\sqrt{n_{//1}^2 - \alpha^2}}{\sqrt{\alpha^2 - 1}}\right) - \frac{2}{\pi}\sqrt{n_{//1}^2 - \alpha^2} \\ &\quad \cdot \mathrm{PV} \int_0^{\infty} \ell n\{q_e(\lambda)\} \frac{d\lambda}{\lambda^2 - (n_{//1}^2 - \alpha^2)}\end{aligned} \tag{34}$$

where for convenience the integration variable is changed from w to λ.

Furthermore, a theoretical verification is again adopted; namely, the absence of the superstrate again leads to the exact expressions obtained in [6], [7].

VI. Thin Dielectric Layers Approximation

Special computer programs are needed in order to calculate the reflection coefficient from the above Sommerfeld-type integrals. Simple, fast, and accurate (for practical applications) expressions are required to be included in microwave integrated circuit (MIC) computer-aided design (CAD) packages. Such an approximation is very usual in practice, and can be obtained considering both dielectric slabs to be electrically thin $k_0 d_1 \ll 1$ and $k_0 d_2 \ll 1$. The authors expand all the above integrands in powers of $k_0 d_i$ and integrating term by term up to $(k_0 d_i)^2$ [terms $(k_0 d_i)^2$ not included]. Following a similar

procedure with that of [9], closed-form expressions for the two functions $\Delta(\alpha)$ and $f_e(\alpha)$ are obtained as

$$\begin{aligned}\Delta(\alpha) &\approx \frac{k_0 d_1 \alpha}{\pi}\left\{\left(\frac{\varepsilon_{//2}}{\varepsilon_{//1}}\cdot\frac{n_{\perp 2}}{n_{//2}}-\frac{\mu_{r1}}{\mu_{r2}}\right)[\ell n(k_0 d_1)+\gamma-1]\right\} \\ &\quad+\left(\frac{1}{\varepsilon_{//1}}-\mu_{r1}\right)\ell n\left(\sqrt{\alpha^2-1}\right) \\ &\quad+\frac{\varepsilon_{//2}}{\varepsilon_{//1}}\cdot\frac{n_{\perp 2}}{n_{//2}}\ell n\left(\frac{n_{\perp 1}}{n_{//1}}\right)+\frac{n_{\perp 1}}{n_{//1}} \\ &\quad\cdot 2Q_0(-\delta_\varepsilon)-2Q_0(\delta_\mu)+\left(1-\frac{n_{\perp 1}}{n_{//1}}\right)\ell n 2\pi \qquad (35)\end{aligned}$$

$$\begin{aligned}&f_e\left(-\sqrt{n_{//1}^2-\alpha^2}\right) \\ &\quad=\frac{-2k_0 d_1}{\pi}\sqrt{n_{//1}^2-\alpha^2}\left\{\frac{\varepsilon_{//2}}{\varepsilon_{//1}}\cdot\frac{n_{\perp 2}}{n_{//2}}\right. \\ &\qquad\cdot\left[\ell n\left(k_0 d_1\frac{n_{\perp 1}}{n_{//1}}\right)+\gamma-1\right] \\ &\qquad\left.+\frac{1}{\varepsilon_{//1}}\ell n\left(\sqrt{\alpha^2-1}\right)+\frac{n_{\perp 1}}{n_{//1}}\cdot[2Q_0(-\delta_\varepsilon)-\ell n 2\pi]\right\} \qquad (36)\end{aligned}$$

where

$$\delta_\varepsilon=\frac{\varepsilon_{\perp 1}\dfrac{n_{\perp 2}}{n_{//2}}-\varepsilon_{\perp 2}\dfrac{n_{\perp 1}}{n_{//1}}}{\varepsilon_{\perp 1}\dfrac{n_{\perp 2}}{n_{//2}}+\varepsilon_{\perp 2}\dfrac{n_{\perp 1}}{n_{//1}}}$$

$$\delta_\mu=\frac{\mu_{r1}-\mu_{r2}}{\mu_{r1}+\mu_{r2}}$$

$$\gamma=0.577\,215\,66\ \ldots \text{ the Euler's constant}$$

and

$$\begin{aligned}Q_0(z)&=\sum_{m=1}^{\infty} z^m \ell n(m) \\ &=\left(\frac{z}{z-1}\right)^2\left\{\ell n 2-\sum_{m=1}^{\infty} z^m \ell n\left[\frac{(m+1)^2}{m(m+2)}\right]\right\}.\end{aligned}$$

An important thing to be noted is that the cover layer thickness $(k_0 d_2)$ is absent from the above expressions. This is because it appears in the expansions only in and above the second-order terms $(k_0 d_2)^2$ or $(k_0 d_1)(k_0 d_2)$, which are, in turn, omitted. This fact means that the reflection coefficient is relatively insensitive from the thickness while it is strongly dependent on the dielectric characteristics of the cover layer, provided of course that the cover layer is electrically thin. In order to account for the cover layer thickness effects, a numerical evaluation of the integrals involved in Γ_{TEM} is necessary.

VII. Surface Waves Approximate Wavenumbers and Turn-On Conditions

The LSE and LSM mode wavenumbers appear as pole singularities in the field or Γ_{TEM} integrals. Their exact location is necessary in order to evaluate these integrals since these poles lie on or near the integration path. An iterative Newton–Raphson scheme is employed for the solution of the corresponding transcendental characteristic (23), (24), (26), (27). A good starting value is needed in this scheme to accelerate convergence but also, and more important, to distinguish the desired solution from the multiple possible solutions. It should be noted at this point that not all of these modes are to be excited, but only those allowed by the two-layer thickness. Thus, the first task is to define the modes which are turned on.

For the single grounded layer, namely the surface modes propagating in the cover layer (for $x > 0$), the turn-on conditions or cutoff frequencies, as well as the approximate wavenumbers, are given in the authors' previous work [7]. It is worth recalling that the first LSE mode is always excited, while the second mode is the first LSM which is turned on when $k_0 d_2\sqrt{n_{\perp 2}^2-1}\geq \pi/2$. Also, the approximate wavenumbers refer to the electrically thin cover layer and its characteristics can be deduced from the corresponding expressions given in [7].

In order to get some practical limits, the cutoff conditions of the grounded double-layer surface waves will be defined. All the field components including the surface waves are proportional to $e^{-k_0 u_0 z}$ in the air region, as shown in (6), where $u_0=\sqrt{\alpha_p^2-1}$. Recalling the radiation condition, $\mathrm{Re}\,(u0)\geq 0$, the valid wavenumbers should have $\alpha_p\geq 1$. Thus, the surface waves cutoff condition is $u_0=0$ or $\alpha_p=1$ while the turn-on, or excitation, condition is $\alpha_p>1$. Letting $u_0=0$ in (26) and (27), the double-layer cutoff conditions for the LSE and LSM modes are obtained in a form similar to that of [10] as shown in the following.

Double layer LSE cutoff condition:

$$\begin{aligned}&\frac{1}{\varepsilon_{\perp 2}}\frac{n_{\perp 2}}{n_{//2}}\sqrt{n_{//2}^2-1}\tan\left\{k_0 d_2\frac{n_{\perp 2}}{n_{//2}}\sqrt{n_{//2}^2-1}\right\} \\ &\quad=-\frac{1}{\varepsilon_{\perp 1}}\frac{n_{\perp 1}}{n_{//1}}\sqrt{n_{//1}^2-1}\tan\left\{k_0 d_1\frac{n_{\perp 1}}{n_{//1}}\sqrt{n_{//1}^2-1}\right\}.\end{aligned} \qquad (37)$$

Double layer LSM cutoff condition:

$$\begin{aligned}&\frac{1}{\mu_{r2}}\sqrt{n_{\perp 2}^2-1}\tan\left\{k_0 d_2\sqrt{n_{\perp 2}^2-1}\right\} \\ &\quad=-\frac{1}{\mu_{r1}}\sqrt{n_{\perp 1}^2-1}\cot\left\{k_0 d_1\sqrt{n_{\perp 1}^2-1}\right\}.\end{aligned} \qquad (38)$$

It is interesting to note that the left-hand side (LHS) of (37) and (38) involves only the superstrate parameters, while the right-hand side (RHS) involves only the substrate parameters. Forcing the absence of the superstrate, e.g., let $d_2=0$, then (37) and (38) reduce to the corresponding cutoff conditions of a single-substrate layer. Similarly, inverting first (38) and forcing the absence of the first layer, e.g., let $d_1=0$, then the single layer-superstrate cutoff conditions are obtained from (37) and (38).

An important observation is that the first solution of (37) is $k_0=0$, thus the first double-layer LSE mode has zero cutoff frequency ($f_c=0$) which means that the LSE_1 is always excited. But, this is not the case for the LSM modes which will be turned on only if the two-layer electrical thickness is adequately high. For a given geometry a graphical representation of (37) and (38) gives the best insight. For this

purpose, and for each one in (37) and (38) separately, the authors can plot one curve versus frequency (versus $k_0 = 2\pi f/c$) for the LHS and another one for the RHS. The cutoff frequencies for each one of the surface-waves modes is defined at the points where the two curves intercept each other.

In most practical applications it is desirable to avoid surface-waves radiation as far as possible. It is thus recommended to select the two-layer thickness to avoid the excitation of the first LSM mode and to retain only the unavoidable LSE_1. For the single-cover layer, this is quite easy because the authors just selected d_2 so that $k_0 d_2 \sqrt{n_{\perp 2}^2 - 1} < \pi/2$. From this, one can see that LSM_1 is more likely to be turned on as d_2 or $n_{\perp 2}$ are increased. Based on this observation one can conclude a safe condition for the double-layer geometry by accounting for a worst case equivalent single layer with thickness $d_{eq} = d_1 + d_2$ and index of refraction $n_{eq} = \max(n_{\perp 1}, n_{\perp 2})$ leading to

Double layer safe condition (non existence of LSM-modes):

$$k_0(d_1 + d_2)\sqrt{\max(n_{\perp 1}^2, n_{\perp 2}^2) - 1} < \frac{\pi}{2}. \tag{39}$$

The condition (39) is similar to that given in [11, p. 160] for the isotropic double-layer case.

As soon as one defines the surface waves which are turned on, their exact wavenumber values are needed for the numerical integration, as explained earlier. Practical situations requires only the two first modes LSE_1 and LSM_1. Approximating both layers to be electrically thin, the corresponding double-layer wavenumbers (denoted with a superscript d) are

$$\alpha_{pe1}^{(d)}\Big|_{k_0 d_i \ll 1} \approx 1 + \frac{1}{2}\left\{\sum_{i=1}^{2} \frac{k_0 d_i}{\varepsilon_{//i}}\left(n_{//i}^2 - 1\right)\right\}^2 \tag{40}$$

$$\alpha_{pm1}^{(d)}\Big|_{k_0 d_i \ll 1} \approx \sqrt{1 + \left(\frac{1}{\sum_{i=1}^{N} \mu_{ri} k_0 d_i}\right)^2} \approx \frac{1}{\sum_{i=1}^{2} \mu_{ri} k_0 d_i}. \tag{41}$$

Equation (40) exactly reduces to that of [11, p. 161] for the isotropic case, while assuming just the absence of the cover layer ($d_2 = 0$) (40) and (41) reduce to those of the authors' previous work [7]. Also, for the single-cover layer the corresponding approximate values $\alpha_{pe1}^{(s)}$ and $\alpha_{pe1}^{(s)}$ result from (40) and (41) by replacing the summation with the term of $i = 2$. Finally, these values are improved employing an iterative Newton–Raphson scheme to solve the characteristic equations.

VIII. Numerical Integration-Singularities

The thin dielectric layers approximation for the reflection coefficient is very fast, but its accuracy is poor and it does not account for the superstrate thickness, even though it remains very useful, especially for the study of microstrip antenna problems where it can be iteratively used in the solution of the corresponding transverse resonance equations. In order to accurately estimate microstrip lines or antenna characteristics the quantities obtained by the thin layers approximation must be improved employing a numerical integration scheme for the reflection coefficient. The same requirement applies also for the investigation of the substrate/superstrate thickness effects.

The semi-infinite integrals involved in the evaluation of the reflection coefficient $\Delta(\alpha)$ and $f_e(\sqrt{n_{//1}^2 - \alpha^2})$ in (31) and (34) possess a number of singularities and branch cuts. In order to avoid the branch cuts the integration path is taken along the $\mathrm{Re}(\lambda)$ axis (from 0 to ∞). The excited LSE surface waves presents poles in the f_e at $\lambda = \pm\lambda_e = \pm\sqrt{\alpha_{pe}^2 - \alpha^2}$, while both LSE and any excited LSM modes present poles in the $\Delta(\alpha)$ integral, the latter at $\lambda = \pm\lambda_m = \pm\sqrt{\alpha_{pm}^2 - \alpha^2}$. It is the usual practice to select the dielectric layers thickness so that no LSM modes are excited. The f_e pole at $\lambda = \sqrt{n_{//1}^2 - \alpha^2}$ has already been taken into account as a Cauchy principal value. Also, the integral $\Delta(\alpha)$ possesses a pair of simple poles at $\lambda = \pm j\alpha$.

Furthermore, the f_e integral possess a number of logarithmic singularities (branch points) for $u_0 = 0$ or at $\lambda = \sqrt{1 - \alpha^2}$ and for $u_{n2}^{(2)} = 0$ or at $\lambda = \sqrt{n_{//2}^2 - \alpha^2}$. The latter singularity appears also in $\Delta(\alpha)$ integral.

Additionally, there are some removable singularities which must be carefully accounted for in order to avoid numerical problems. In both integrals the term $\tanh[k_0 d_1 u_{n2}^{(1)}]/u_{n2}^{(1)}$ is replaced by $k_0 d_1$ in the limit when $u_{n2}^{(1)} \to 0$. Also, in $\Delta(\alpha)$ two terms of the form $u_{n1}^{(i)} \coth[k_0 d_i u_{n1}^{(i)}]$ for $i = 1, 2$ appear within D_{LSM}, which are replaced by $1/k_0 d_i$ in the limit when $u_{n1}^{(i)} \to 0$.

Depending on the value of the propagation constant $\alpha = n_{//1} \sin\phi$ (or the angle of incidence) some of these singularities may be located on the integration path $\mathrm{Re}(\lambda)$ axis, or they may be moved away on the $\mathrm{Im}(\lambda)$ axis where they do not affect the numerical integration. As explained in the authors' previous work [7] one can distinguish three cases and for each of them the integration path is properly modified. The definition of each case is as follows:

1) $\alpha_{pe1}^{(s)} < \alpha_{pe1}^{(d)} < \alpha < n_{//1}$ is the total reflection case;
2) $1 < \alpha < \alpha_{pe1}^{(s)}$ when there is only surface waves excitation;
3) $0 < \alpha < 1$ when there are both surface waves and sky wave radiation (the edge radiates, thus it works as an antenna).

For the integrals' numerical evaluation the integration path is subdivided into proper unequal small sections, when the singularities are first located on the $\mathrm{Re}(\lambda)$ axis. The integration is performed up to a point close to the singularity and then resumes just after it. The relatively slowly varying logarithmic singularities (λ_0) are approached up to $(1 \pm 10^{-5})\lambda_0$ while the faster varying pole singularities (λ_p) up to $(1 \pm 10^{-4})\lambda_p$. Also, the subintervals are selected to become gradually smaller as a singularity is approached. Furthermore, more subintervals are taken up to the point $\lambda = \max(n_{\perp i}, n_{//i})$, $i = 1, 2$. When these intervals are

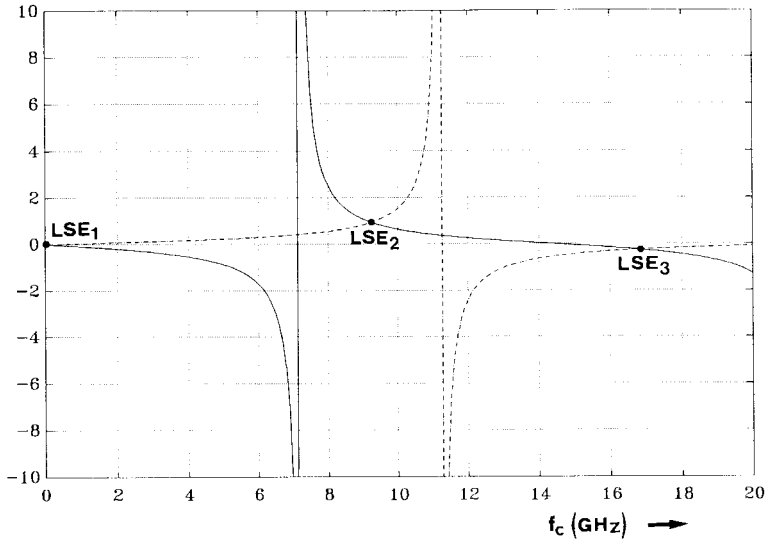

(a)

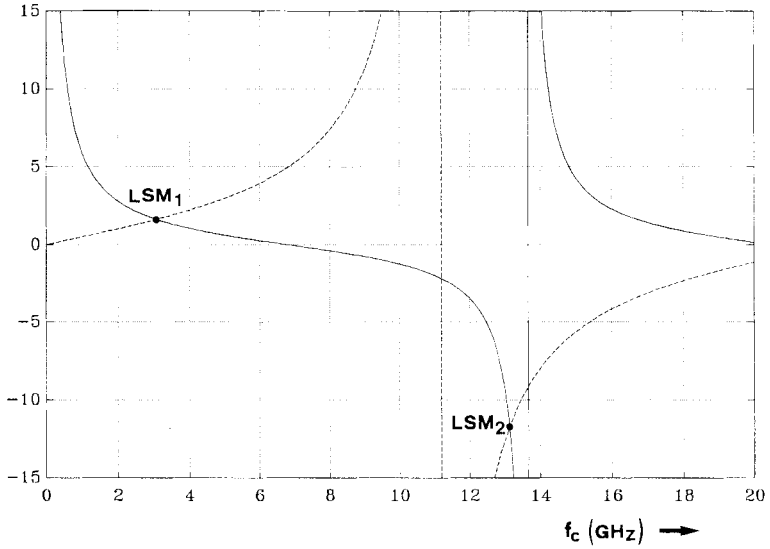

(b)

Fig. 3. Graphical solution of the double-layer cutoff conditions for a PTFE substrate and Epsilam-10 superstrate. (a) LSE-modes, (37). (b) LSM modes, (38).

established and are put in an increasing order an adaptive Romberg integration with an error tolerance 10^{-6} is performed in each of them. For the remaining semi-infinite interval, a progressive Romberg integration, on subintervals with length $\min(1/k_0 d_i)$ is performed until the last contribution becomes less than 10^{-5}.

IX. A Rectangular Microstrip Antenna with a Cover Layer

In the authors' previous work [14] closed-form expressions for the field under the radiating patch, the resonant frequency or the resonant length, and the input impedance of a probe fed rectangular patch antenna has been given. These expressions can be modified for the present case, essentially using the above-given reflection coefficient. The two transverse resonant conditions are

$$\left.\begin{aligned} X(\alpha) - k_0 \ell \sqrt{n_{//1}^2 - \alpha^2} &= -p\pi \\ X\left(\sqrt{n_{//1}^2 - \alpha^2}\right) - k_0 h \alpha &= -q\pi \end{aligned}\right\}, \quad \text{with} \quad p, q = 0, 1, 2, \cdots \tag{42}$$

where ℓ and h are the dimensions of the patch, respectively.

The resonant frequency can be calculated from (42) following the procedure described in [6]. The resonant length of the antenna can be found by solving the first of (42) to establish a transverse resonance for a fixed width ℓ and fixed frequency f. The resulting propagation constant α_p is used in the second of (42) and the resonant length h considering the excitation of a TMqp mode is

$$\frac{h_{\text{res}}}{\lambda} = \frac{X\left(\sqrt{n_{//1}^2 - \alpha^2}\right) + q\pi}{2\pi\alpha_p}. \tag{43}$$

Similarly, the microstrip antenna input impedance can be obtained by substituting the above developed reflection coefficient into the expressions given in [6], [14].

X. Numerical Results and Discussions

The first concern is the examination of the surface waves turn-on conditions and their wavenumbers. A MATLAB program was written for the graphical presentation of the double-layer cutoff conditions (37), (38) versus frequency. An example is shown in Fig. 3, for which the same data used in [10] are adopted for comparison purposes, where a Teflon (PTFE) substrate with $\varepsilon_{\perp 1} = 2.88$, $\varepsilon_{//1} = 2.43$, $d_1 = 8.02$ mm, and Epsilam-10 superstrate with $\varepsilon_{\perp 2} = 13$, $\varepsilon_{//2} = 10.3$, $d_2 = 1.95$ mm are assumed. The two curves shown in Fig. 3(a) correspond to the LHS and RHS of (37) and their intercept points define the LSE cutoff frequencies approximated as $f_{c1} = 0$, $f_{c2} = 9.22$ GHz, and $f_{c3} = 16.9$ GHz. Similarly, Fig. 3(b) corresponds to (38) and the LSM cutoff frequencies are $f_{c1} = 3.07$ GHz, $f_{c2} = 13.14$ GHz. These results are almost identical to those in [10] where the corresponding equations were solved numerically. The authors' graphical presentation offers a simple and clear insight into the entire situation.

Having estimated the cutoff frequencies it is then clear which surface modes are excited. The authors will deal with the usual case when only the first LSE modes are excited. The dependence of the substrate and superstrate thickness on the wavenumbers $\alpha_{pe1}^{(s)}$ and $\alpha_{pe1}^{(d)}$ for both the single (cover) and double grounded layer are of special interest. A Newton–Raphson iterative scheme is employed for the solution of (23) and (26). The authors start from the approximate values of the wavenumbers given in (40). It must be kept in mind that their exact value is required in the numerical integration, thus an error tolerance of the order of 10^{-6} is demanded. A parametric investigation for both $\alpha_{pe1}^{(s)}$ and $\alpha_{pe1}^{(d)}$ versus the superstrate thickness (d_2/λ) with the horizontal dielectric constant $(\varepsilon_{\perp 2})$ of the cover layer as a parameter, is shown in Fig. 4. It can be concluded that is always $\alpha_{pe1}^{(d)} \backslash \alpha_{pe1}^{(s)}$ while both of them are increased when $\varepsilon_{\perp 2}$ is increased.

Epsilam-10 is considered for the substrate and PTFE for the superstrate in Fig. 4(a), while these are assumed vice versa in Fig. 4(b). Higher values are obtained in Fig. 4(b), because the superstrate has high dielectric constant (Epsilam-10) and its thickness is increased while it is considered thin in Fig. 4(a). It is first observed that the anisotropy effects become significant only for electrically thick substrates in terms of $d\sqrt{\varepsilon_r}/\lambda_0$ rather than d/λ_0. Recall that the condition for surface-wave excitation only, without sky wave radiation, is $1 < \alpha = n_{//1} \sin\varphi < \alpha_{pe1}^{(d)}$. Also, note that $\alpha_{pe1}^{(d)}$ [and $\alpha_{pe1}^{(s)}$] may become quite higher than unity [even $\alpha_{pe1}^{(d)} \to 2$] for thick layers, as in the case of Fig. 4(b) for example. It is then concluded that thick layers (either sub- or superstrate) with high dielectric constant may lead to excessive surface-wave coupling and even without sky-wave radiation. This situation must be avoided, especially in microstrip antennas, where sky wave is the useful radiation while surface waves only give rise to power losses. Thus, such a structure will act as a questionable antenna.

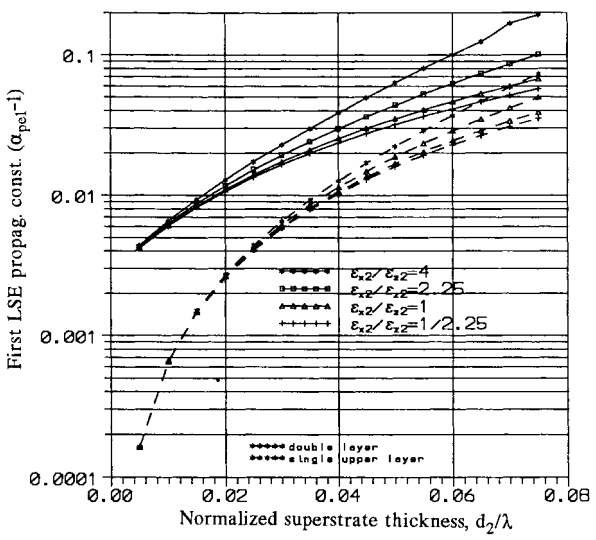

(a)

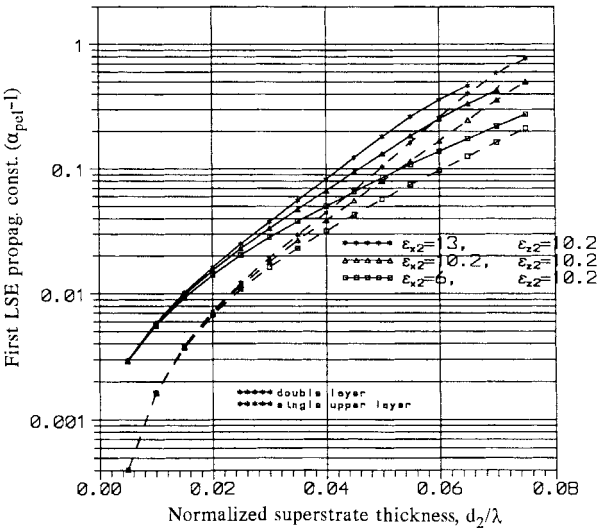

(b)

Fig. 4. Propagation constant of the first single and double-layer LSE mode. Actually, $[\alpha_{pe1}^{(s)} - 1]$ and $[\alpha_{pe1}^{(d)} - 1]$ versus the normalized superstrate thickness (d_2/λ) with $\varepsilon_{\perp 2}$ as a varied parameter. (a) Substrate is Epsilam-10 and superstrate is PTFE and (b) vice versa.

The incident TEM-wave reflection coefficient (Γ), for a practical case of electrically thin substrate (Epsilam-10) and thin superstrate (PTFE), versus the angle of incidence φ (or the propagation constant $\alpha = n_{//1} \sin\varphi$) with the superstrate anisotropy ratio ($n_{\perp 2}/n_{//2} = 2, 1.5, 1, 1/1.5$) as a parameter, is shown in Fig. 5. The agreement between the thin layers approximation and the numerical integration is quite good for the phase of Γ given by $\mathrm{Re}\{x(\alpha)\}$ with an error less than about 8%, but the agreement is rather poor for the magnitude of Γ given by $\exp[-\mathrm{Im}\{x(\alpha)\}]$ with an error up to about 25%. Also, the thin layers approximation does not account for the superstrate anisotropy in the $\mathrm{Im}\{x(\alpha)\}$. Moreover, the behavior of $X(\alpha)$ in this case, namely when the substrate dielectric constants are higher than those of

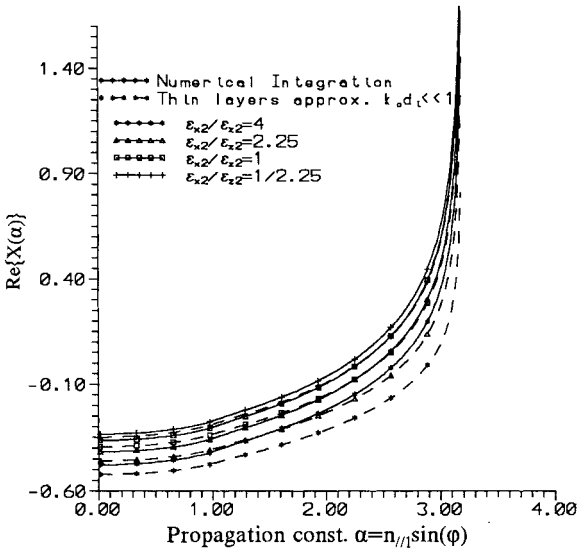

(a)

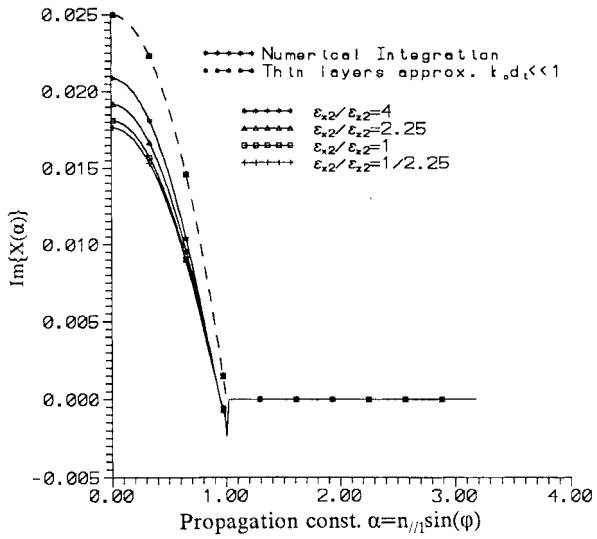

(b)

Fig. 5. Influence of the superstrate dielectric anisotropy on the reflection coefficient and comparison of the thin layers approximation with the numerical integration. (a) Phase of the reflection coefficient $\arg(\Gamma) = \mathrm{Re}\{x(\alpha)\}$. (b) Magnitude of the reflection coefficient $|\Gamma| = \exp[-\mathrm{Im}\{x(\alpha)\}]$.

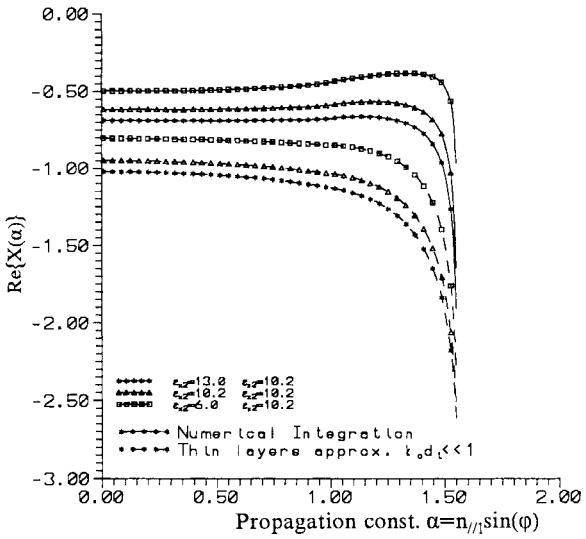

(a)

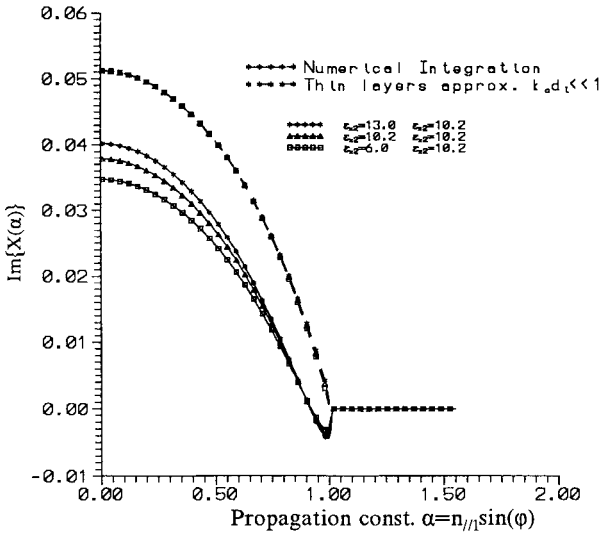

(b)

Fig. 6. Effects of the superstrate dielectric anisotropy on the reflection coefficient when the superstrate (Epsilam-10) has higher dielectric constant than the substrate (PTFE). (a) $\mathrm{Re}\{x(\alpha)\}$ and (b) $\mathrm{Im}\{x(\alpha)\}$.

the superstrate, is quite similar to that without a superstrate examined in the authors' previous work [7]. A similar investigation is shown in Fig. 6 where PTFE substrate and Epsilam-10 superstrate are used. It is important to note that an inversion in the behavior of the $\mathrm{Re}\{x(\alpha)\}$ occurs, (it tends to negative values instead of positive as α is increased) and this is due to the fact that the superstrate dielectric constants are higher than those of the substrate. This phenomenon has major effects on the conditions required for the establishment of a transverse resonance in microstrip antennas. Moreover, even though the variation of the superstrate anisotropy ratio $(n_{\perp 2}/n_{//2})$ is quite smaller than that of the previous case (Fig. 5), the deviation between thin layers approximation and numerical integration is quite larger. From a closer examination one can see that the same superstrate physical thickness is used in the two cases (Figs. 5 and 6) but the actual electrical thickness is proportional to the effective index of refraction. So, one can say that in Fig. 6 the thickness is approximately increased by the ratio of (Epsilam $n_{//}$)/(PTFE $n_{//}$) which is $\sqrt{10.2/2.43} \approx 2$ and the actual electrical thickness $k_0\sqrt{\varepsilon_{//}}d_2$ is about 0.2 and 0.4, respectively.

The effects of the superstrate thickness (d_2/λ) on the reflection coefficient are investigated in Fig. 7 for a case with an Epsilam substrate and PTFE superstrate. The thin layers approximation accounts for the superstrate anisotropy ratio only for the phase of the $\arg(\Gamma) = \mathrm{Re}\{x(\alpha)\}$ as shown in Fig. 7(a), but fails to account for it when its magnitude $|\Gamma| = \exp[-\mathrm{Im}\{x(\alpha)\}]$ is concerned [Fig. 7(b)]. Also, as shown in Fig. 7(a) and (b), the thin layers approximation fails to account for the superstrate thickness for both $\arg(\Gamma)$ and

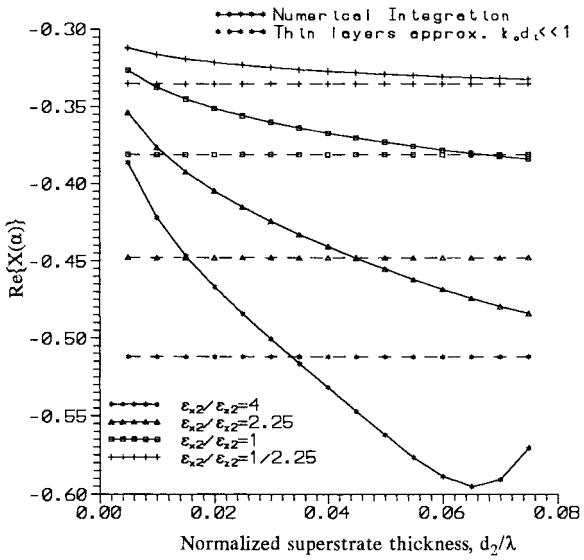

(a)

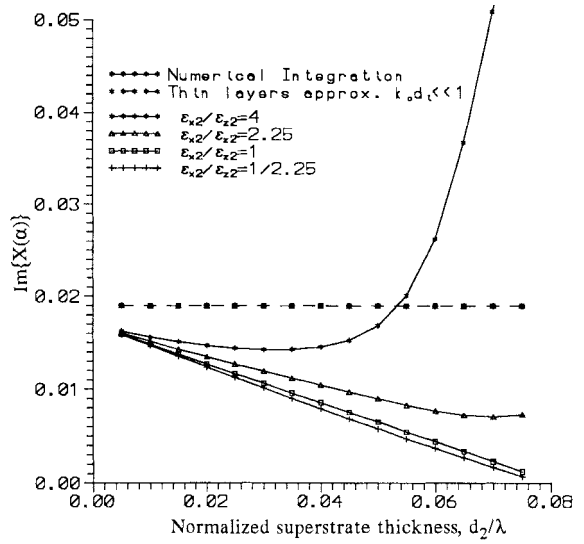

(b)

Fig. 7. Effects of the superstrate thickness on the reflection coefficient $\Gamma(\alpha)$ when $\alpha = n_{//1} \sin \varphi = 0.5$ with the superstrate anisotropy ratio as a parameter. (a) $\mathrm{Re}\{x(\alpha)\}$ and (b) $\mathrm{Im}\{x(\alpha)\}$.

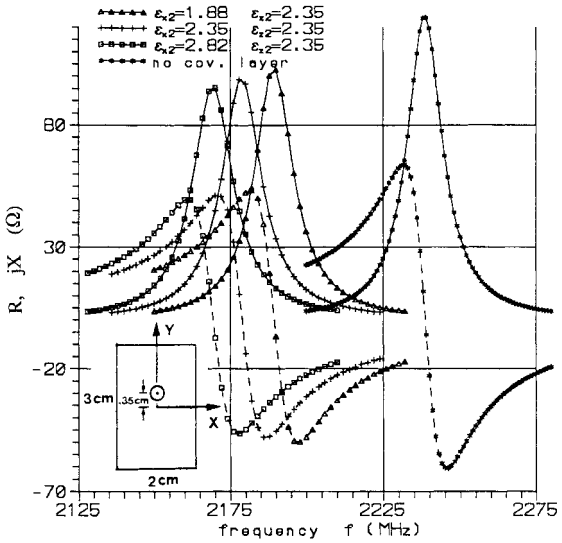

(a)

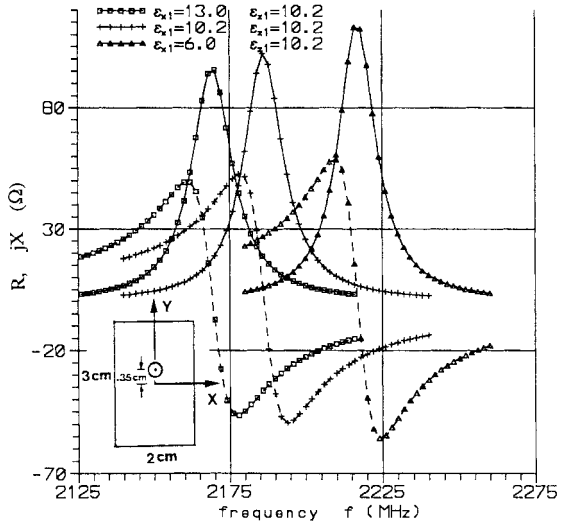

(b)

Fig. 8. Effects of the dielectric anisotropy on a rectangular patch antenna printed on Epsilam-10 with PTFE cover layer, when the anisotropy ratio of (a) superstrate and (b) substrate is varied.

$|\Gamma|$. Moreover, both $\mathrm{Re}\{x(\alpha)\}$ and $\mathrm{Im}\{x(\alpha)\}$ are, in general, decreased when d_2/λ is increased. This corresponds to a decrease of $\arg(\Gamma)$ but to an increase of $|\Gamma|$. An exception in this behavior of $\mathrm{Re}\{x(\alpha)\}$ is observed for high d_2/λ and high $\varepsilon_{\perp 2}$ as shown in Fig. 7(a) for $\varepsilon_{\perp 2}/\varepsilon_{//2} = 4$. This seems to be due to the excitation of the first LSM mode. The first LSM turn-on condition for the single-cover layer is $2\pi\sqrt{\varepsilon_{\perp 2} - 1}d_2/\lambda_0 < \pi/2$ and for the double layer is $2\pi\sqrt{\varepsilon_{\perp 1} - 1}(d_1/\lambda_0 + d_2/\lambda_0) < \pi/2$ since $\varepsilon_{\perp 1} > \varepsilon_{\perp 2}$. For the data assumed in Fig. 7(a) ($\varepsilon_{\perp 1} = 13$, $\varepsilon_{\perp 2} = 9.4$, $\lambda_0 = 10$ cm) there is not any single-cover layer LSM excitation since the $\mathrm{LSM}_1^{(s)}$ is excited for $d_2/\lambda_0 > 0.09$, but it is possible for the double-layer $\mathrm{LSM}_1^{(d)}$ to be excited for $d_2/\lambda_0 \geq 0.06$. This actually occurred for the curve $\varepsilon_{\perp 2}/\varepsilon_{//2} = 4$ and $d_2/\lambda_0 \geq 0.065$.

Further examination of Fig. 7(b) shows that a steep increase in $\mathrm{Im}\{x(\alpha)\}$ corresponding to a steep decrease in $|\Gamma|$ is observed for $\varepsilon_{\perp 2}/\varepsilon_{//2} = 4$ and superstrate thickness d_2/λ_0 greater than about 0.04. This must be due to a strong coupling of energy-to–surface-wave modes. A similar behavior was observed without the cover layer, [7], when the substrate thickness was increased over about $d_1/\lambda_0 \geq 0.04$ and for high $\varepsilon_{\perp 1}$. Also, the effects of increasing the superstrate thickness (d_2/λ) on the reflection coefficient are much lower (by a factor of about 10) than the effects of increasing the substrate thickness without the cover layer [7]. The same conclusion is true when a cover layer is present.

The input impedance for the dominant mode (TM_{10}) of a rectangular patch antenna printed on Epsilam-10 with a PTFE cover layer is shown in Fig. 8. The substrate anisotropic dielectric constant is kept constant in Fig. 8(a) while the cover layer anisotropy ratio $(\varepsilon_{\perp 2}/\varepsilon_{//2})$ is varied through its

practically occurring values. The resonant frequency as well as the resonant impedance are drastically lowered when the cover layer is present, while a further decrease is observed as the $\varepsilon_{\perp 2}$ is increased from 1.88 to 2.82. Similar behavior is observed in Fig. 8(b) where a fixed uniaxial superstrate is assumed and the substrate anisotropy ratio $(\varepsilon_{\perp 1}/\varepsilon_{//1})$ is varied. Namely, the resonant frequency and the resonant impedance are lowered as $\varepsilon_{\perp 1}$ is increased. In both cases, major effects are observed, thus the presence of the cover layer as well as the two layers anisotropy should be taken into account during the design. Otherwise, the antenna may be operating completely outside the frequency band for which it was intended.

XI. Conclusion

A Wiener–Hopf-type technique in conjunction with a space-domain Fourier transform was employed to solve the canonical problem of TEM wave obliquely incident upon the edge of a semi-infinite plate conductor lying at the interface of two uniaxial dielectrics, which form an otherwise grounded double-layer geometry. The single cover layer and double-layer LSE and LSM modes characteristic equations, along with their cutoff conditions, and the techniques to solve them, were given. An electrically thin layer approximation and semi-infinite integration was carried out for the Sommerfeld-type integrals involved within the reflection-coefficient expressions. A twofold theoretical verification was adopted for all the analytical expressions obtained by forcing the absence of the superstrate or considering both layers to be isotropic and verifying the expressions of [7] and [4], respectively. Numerical investigations have shown that the presence of the superstrate, as well as both layers' dielectric anisotropy, cause significant effects on the characteristics of microstrip lines or patch antennas printed in such a geometry. It is also concluded that numerical integration should be employed in the case of thick layers, but the thin layers approximation is of primary importance in the solution of patch-antennas transverse–resonance equations. The present analysis can also be used for the examination of quite interesting possibilities like substrate–superstrate resonant thickness first proposed in [1]–[3] by further extending the numerical integration scheme.

References

[1] D. R. Jackson and N. G. Alexopoulos, "Analysis of planar strip geometries in a substrate-superstrate configuration," *IEEE Trans. Antennas Propagat.*, vol. AP-34, pp. 1430–1438, Dec. 1986.

[2] N. G. Alexopoulos and D. R. Jackson, "Fundamental superstrate (cover) effects on printed circuit antennas," *IEEE Trans. Antennas Propagat.*, vol. AP-32, pp. 807–815, Aug. 1984.

[3] D. R. Jackson and N. G. Alexopoulos, "Gain enhancement methods for printed circuit antennas," *IEEE Trans. Antennas Propagat.*, vol. AP-33, pp. 976–987, Sept. 1985.

[4] Y. Tu and D. C. Chang, "Effect of a cover layer on the edge admittance of a wide microstrip," *IEEE Trans. Antennas Propagat.*, vol. 39, pp. 354–358, Mar. 1991.

[5] G. A. Kyriacou and J. N. Sahalos, "Effect of substrate-superstrate uniaxial anisotropy on microstrip structures," *Electron. Lett.*, vol. 30, no. 19, pp. 1557–1558, Sept. 1985.

[6] ——, "The edge admittance model for the study of microstrips on uniaxial substrate," *Archiv. fur Elektrotech.*, vol. 76, pp. 169–179, 1993.

[7] ——, "A Wiener–Hopf type analysis of microstrips printed on uniaxial substrates: Effect of the substrate thickness," *IEEE Trans. Microwave Theory Tech.*, vol. 43, pp. 1967–1977, Aug. 1995.

[8] R. Mittra and S. W. Lee, *Analytical Techniques in the Theory of Guided Waves.* New York: Macmillan, 1971.

[9] E. F. Kuester, R. T. Johnk, and D. C. Chang, "The thin substrate approximation for reflection from the end of a slab-loaded parallel-plate wave waveguide with application to microstrip patch antennas," *IEEE Trans. Antennas Propagat.*, vol. AP-30, pp. 910–917, Sept. 1982.

[10] Peixeiro and A. M. Barbosa, "Leaky and surface waves in anisotropic printed antenna structures," *IEEE Trans. Antennas Propagat.*, vol. 40, pp. 566–569, May 1992.

[11] J. R. Mosig, "Numerical techniques for microwave and millimeter wave passive structures," in *Integral Equation Techniques*, T. Itoh, Ed. New York: Wiley, 1989, ch. 3.

[12] MATLAB for Windows, version 4.2b, © The Mathworks, Inc., South Nadick, MA.

[13] D. C. Chang and E. F. Kuester, "Total and partial reflection from the end of a parallel-plate waveguide with an extended dielectric slab," *Radio Sci.*, vol. 16, no. 1, pp. 1–13, 1981.

[14] G. Kyriacou and J. N. Sahalos, "An easy to use method to define the input impedance of a probe-fed rectangular microstrip antenna," in *Archiv. fur Elektrotech. 70.* Berlin, Germany: Springer-Verlag, 1987, pp. 349–357.

[15] D. C. Chang, "Analytical theory of an unloaded rectangular microstrip patch," *IEEE Trans. Antennas Propagat.*, vol. AP-29, pp. 54–62, Jan. 1981.

[16] R. E. Collins, *Field Theory of Guided Waves.* Piscataway, NJ: IEEE Press, 1991.

George A. Kyriacou (M'90) was born in Famagusta, Cyprus, on March 25, 1959. He received the Electrical Engineering Diploma and the Ph.D. degree, both with honors, from Demokritos University of Thrace, Xanthi, Greece, in 1984 and 1988, respectively.

Since January 1990, he has been a Lecturer at the Microwaves Laboratory, Demokritos University of Thrace, where he is now an Assistant Professor. His current research interests include microwave engineering, antennas, applied electromagnetics, and biomedical engineering. He works on electrical impedance tomography and participates in several European Union programs.

Dr. Kyriacou is a member of the Technical Chamber of Greece.

John N. Sahalos (M'75–SM'84) was born in Philippiada, Greece, in November 1943. He received the B.Sc. degree in physics and the Diploma in civil engineering from the University of Thessaloniki, Thessaloniki, Greece, in 1967 and 1975, respectively, as well as the Ph.D. in electromagnetics and the Diploma of Post-Graduate Studies in 1974 and 1975, respectively, from the same university.

From 1971 to 1974, he was a Teaching Assistant of physics at the University of Thessaloniki, as well as an Instructor from 1974 to 1976. During 1976, he worked at the ElectroScience Laboratory, Ohio State University, Columbus, as a Post-Doctoral Fellow. From 1977 to 1985, he was a Professor in the Electrical Engineering Department, University of Thrace, Greece, and Director of the Microwaves Laboratory. During 1982, he was a Visiting Professor at the Department of Electrical and Computer Engineering, University of Colorado, Boulder. Since 1985, he has been a Professor at the School of Science, University of Thessaloniki, Greece, where he is the leader of the Radiocommunications Group. During 1989, he was a Visiting Professor at the Universidat Politechnica de Madrid, Madrid, Spain. He is the author of three books and more than 190 articles published in the scientific literature. His research interests are in the area of applied electromagnetics, antennas, high-frequency methods, communications, microwaves, and biomedical engineering.

Dr. Sahalos is a Professional Engineer and a Consultant to industry. He has been honored with the Investigation Fellowship of the Ministerio de Education Y Ciencia (Spain). Since 1985, he has been a member of the Editorial Board of the IEEE Transactions on Microwave Theory and Techniques. Since 1992, he has been a member of the URSI Commissions A and E. He is also a member of five IEEE Societies, the New York Academy of Science, and the Technical Chamber of Greece.